Radiative convective flow of MHD hybrid nanofluid over a inverted cone with porous medium

S. Munirathinam [a], S. Kirusakthika [b], M. Kayalvizhi [c], B. Ganga [d], A.K. Abdul Hakeem [b,*]

[a] Department of Mathematics, Sri Vidya Mandir Arts and Science College, Uthangarai – 636 902, India.

[b] Department of Mathematics, Sri Ramakrishna Mission Vidyalaya College of Arts and Science, Coimbatore - 641 020, India.

[c] Department of Mathematics, Government Polytechnic, Daman – 396 210.

[d] Department of Mathematics, Providence College for Women, Coonoor – 643 104, India.

drabdulmaths@gmail.com

Article History: Received: 15-05-2023 **Revised:** 16-06-2023 **Accepted:** 27-06-2023

Abstract

An analysis of a MHD hybrid based nanofluid flow past a spinning cone with thermal radiation embedded in a porous medium. In this study, we consider Casson fluid model for the behavior of non – Newtonian fluid. Here, we chose Al_2O_3 – TiO_2, TiO_2 – Cu and Al_2O_3 – Cu hybrid nanoparticles with Newtonian and non–Newtonian base fluids. Formulated governing expressions are comprehend by implementing similarity transformations and numerically solved by an shooting scheme utilizing an Fourth-order Runge-Kutta procedure. The significance of relevant parameters are inquired in the form of plots and tables. By varying the wide values of radiation parameter and magnetic parameter, the temperature profile is mounted. Besides, tangential velocity field escalated with spin parameter and Darcy parameter. An increment in the range of pertinent variables indicates that the increase in the Skin friction coefficient of sodium alginate based hybrid nanofluid, whereas reverse trend is seen in heat transfer rate. That is, water based hybrid nanofluid is enhanced.

Keywords: Hybrid, cone, magnetic field, Casson fluid, thermal radiation, porous medium.

1. Introduction

The dissection of heat change in diverse fluids past a spinning cone is important due to its industrial and engineering applications including of food processing technology, manufacturing of transmission missile gun, endoscopy scanning etc. The flow of porous media is applied in packed filters, pebble – type heat exchanger, geothermal operations and petroleum reservoirs. Natural convective flow over a spinning cone embedded in anisotropic permeable media has been studied by Beg [1]. The concept of radiative heat exchange played a role in industrial because temperature will be high in their processes and also significance in agriculture, archaeology, space exploration, generating electricity. Sambath [2] evaluated chemical reaction on the unsteady flow due to MHD radiative natural convective transport system over a vertical surface. Makanda [3] and Mallikarjuna [4] discussed the radiation effect in a spinning cone with non – Darcy porosity regime. Analysis of peristaltic motion of Sisko fluid with entrophy generation has been done by Hayat [5]. Combined non – linear convection and porosity was examined by Raju [6] and Mohana Raju [7] past a revolving cone. The heat transport of radiation has been considered in [8 – 10] with various flow regimes of mathematical models.

Nanofluids are a type of fluids which contains a nanometer size particles (diameter < 100nm) are dispersed in a convectional base fluids. This new study has motivated many researches in industrial sector. Moreover in nanofluid, it has many applications such as damaging of cancer cells, solar systems, heat exchangers and so on. The suspension of two or more nanoparticles are blended in a single base fluid called Hybrid nanofluids which enhances the heat transfer than nanofluids and used in drug reduction, vehicle thermal co-ordination, refrigeration and aeronautical device making, etc. Hamida [11] used finite element method in COMSOL Multiphysics software to consider the nanofluid flow is induced by the square cavity. The numerical results gave the impression that the Ethylene glycol – Cu nanofluid enhances the heat transfer than other nanoparticles, which depends strongly on nano – thermal conductivity. AbdulHakeem [12] and Ganga [13] presented the radiative convective flow in a stretching sheet. Alwawi [14] evaluated Casson fluid past a solid sphere for MHD convective flow with constant surface heat flux. Ragupathi [15] illustrated non – Darcy nanofluids in a riga plate by dispersing magnetite (Fe_3O_4) and aluminium oxide (Al_2O_3) nanoparticles in water and sodium alginate. Khan [16] and Raju [17] studied rotating disk along with radiation effects.

Jamaludin [18] inspected MHD mixed convective flow of hybrid nanofluid over a stretching / shrinking sheet. Hussanan [19] tested the impact of viscous dissipation in MHD boundary layer flow of Casson hybrid nanofluid. They concluded that sodium alginate based hybrid nanofluid have high rates of heat transfer. Yusuf [20] highlighted three directional flows of Darcy – Forchheimer hybrid nanofluid with non – linear thermal radiation and remarked that temperature is increased with porosity. Hosseinzadeh [21] employed the radiative MHD hybrid nanofluid in a vertical cylinder and also studied different shape factors. Entropy analysis in MHD flow on a cone with porosity effect is worked out by Hanif [22]. Further investigation related to cone models are reviewed in [23 - 25].

Keeping the view in the above mentioned studies, the current study is the outcome of heat transfer analysis of MHD radiative hybrid nanofluid with porous medium over an inverted rotating cone. The governing models are deduced to system of ODE using suitable transformations and solved numerically by adopting bvp4c in Matlab. The impact of heat and flow features are deliberated. Table 1 displays the properties for base fluids H_2O, $NaC_6H_9O_7$ with nanoparticles Al_2O_3 , TiO_2 , Cu.

Table 1 Thermophysical properties [15,18].

Properties	C_p/(J/(kg.K))	ρ/(kg/m^3)	k/(W/(m.K))	β/10^{-5}(1/K)	σ(sm^{-1})
H_2O	4179	997	0.613	21	0.05
$NaC_6H_9O_7$	4175	989	0.6376	99	$2.6\text{x}10^{-4}$
Al_2O_3	765	3970	40	0.85	$3.5\text{x}10^{7}$
TiO_2	686.2	4250	8.954	0.9	$2.38\text{x}10^{6}$
Cu	385	8933	400	1.67	$5.96\text{x}10^{7}$

2. Mathematical Formulation:

This problem elucidated the stream of MHD, laminar, incompressible and two dimensional natural convective Darcy flow of Water (H_2O) and Sodium Alginate ($NaC_6H_9O_7$) as base fluids with three different hybrid nanoparticles (Aluminum Oxide (Al_2O_3), Titanium Oxide (TiO_2), Copper (Cu)) over a rotating vertical cone as displayed in Fig.1. Here y*- direction connected normal to the cone surface and x*- direction measured along the cone surface. Ω is the constant angular speed of the cone about the vertical symmetry axis. Under a boundary layer approximations are mentioned as follows [1,22,23]:

$$\frac{\partial}{\partial x^*}(r^* u^*) + \frac{\partial}{\partial y^*}(r^* v^*) = 0\,, \tag{1}$$

$$\rho_{hnf}\left(u^*\frac{\partial u^*}{\partial x^*} + v^*\frac{\partial u^*}{\partial y^*} - \frac{w^{*2}}{x^*}\right) = \left(1+\frac{1}{\beta}\right)\mu_{hnf}\frac{\partial^2 u^*}{\partial y^{*2}} + (\rho\beta_T)_{hnf}\,g\cos\gamma(T-T_0) - \frac{\mu_{hnf}}{K}u^* - \sigma_{hnf}B^2u^*\,, \tag{2}$$

$$\rho_{hnf}\left(u^*\frac{\partial w^*}{\partial x^*} + v^*\frac{\partial w^*}{\partial y^*} + \frac{u^* w^*}{x^*}\right) = \left(1+\frac{1}{\beta}\right)\mu_{hnf}\frac{\partial^2 w^*}{\partial y^{*2}} - \frac{\mu_{hnf}}{K}w^* - \sigma_{hnf}B^2 w^*, \tag{3}$$

$$(\rho C_p)_{hnf}\left(u^*\frac{\partial T}{\partial x^*} + v^*\frac{\partial T}{\partial y^*}\right) = k_{hnf}\frac{\partial^2 T}{\partial y^{*2}} - \frac{\partial q_r}{\partial y^*}\,, \tag{4}$$

The following boundary conditions are [1]

$$u(x^*,0) = 0, \quad v(x^*,0) = 0, \quad w(x^*,0) = r^*, \quad T(x^*,0) = T_0 + (T_r - T_0)\frac{x^*}{L}\,, \tag{5}$$

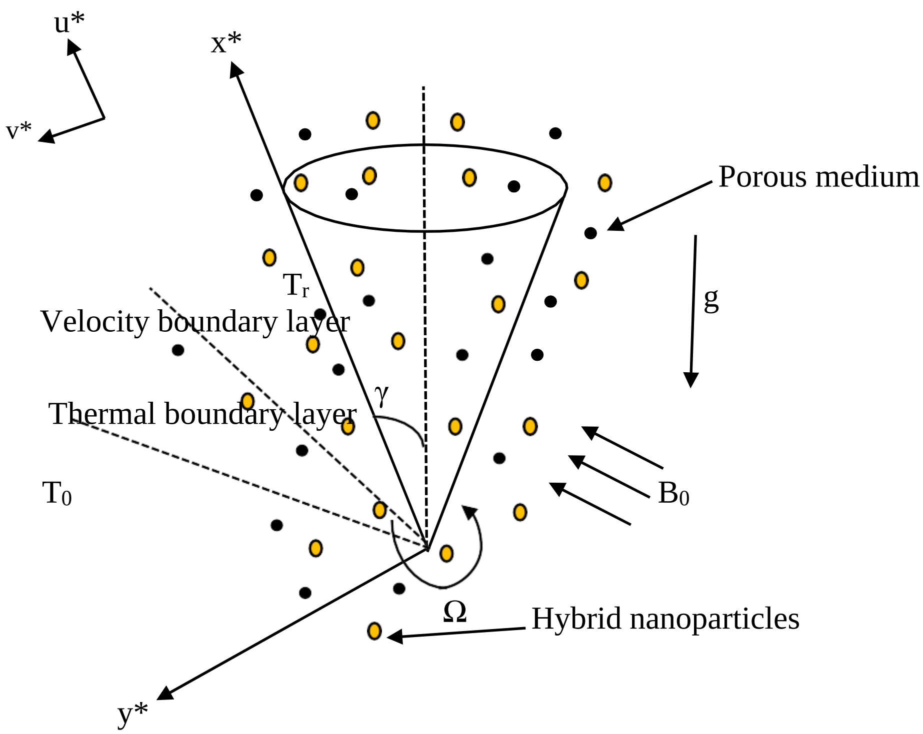

Fig. 1 Geometry of the problem.

The hybrid nanofluid properties are given by [22]

$$\mu_{hnf} = \frac{\mu_f}{(1-\phi_1)^{2.5}(1-\phi_2)^{2.5}} , \qquad (6)$$

$$\rho_{hnf} = \{(1-\phi_2)[(1-\phi_1)\rho_f + \phi_1\rho_{s_1}]\} + \phi_2\rho_{s_2} , \qquad (7)$$

$$\alpha_{hnf} = \frac{k_{hnf}}{(\rho C_p)_{hnf}} , \qquad (8)$$

$$(\rho C_p)_{hnf} = \{(1-\phi_2)[(1-\phi_1)(\rho C_p)_f + \phi_1(\rho C_p)_{s1}]\} + \phi_2(\rho C_p)_{s2} , \qquad (9)$$

$$(\rho\beta_T)_{hnf} = \{(1-\phi_2)[(1-\phi_1)(\rho\beta_T)_f + \phi_1(\rho\beta_T)_{s_1}]\} + \phi_2(\rho\beta_T)_{s_2} , \qquad (10)$$

$$\frac{k_{hnf}}{k_{nf}} = \frac{k_{s_2} + 2k_{nf} - 2\phi_2(k_{nf} - k_{s_2})}{k_{s_2} + 2k_{nf} + \phi_2(k_{nf} - k_{s_2})} , \qquad (11)$$

where

$$\frac{k_{nf}}{k_f} = \frac{k_{s_1} + 2k_f - 2\phi_1(k_f - k_{s_1})}{k_{s_1} + 2k_f + \phi_1(k_f - k_{s_1})} ,$$

$$\frac{\sigma_{hnf}}{\sigma_{nf}} = \frac{\sigma_{s_2} + 2\sigma_{nf} - 2\phi_2(\sigma_{nf} - \sigma_{s_2})}{\sigma_{s_2} + 2\sigma_{nf} + \phi_2(\sigma_{nf} - \sigma_{s_2})} , \qquad (12)$$

where

$$\frac{\sigma_{nf}}{\sigma_f} = \frac{\sigma_{s_1} + 2\sigma_f - 2\phi_1(\sigma_f - \sigma_{s_1})}{\sigma_{s_1} + 2\sigma_f + \phi_1(\sigma_f - \sigma_{s_1})} ,$$

In the above, the suffix s_1, s_2 denotes the solid nanoparticles and ϕ_1, ϕ_2 are the solid volume fraction. Therefore, in this model 0.5% and 1.5% solid volume fraction ($\phi_1$and ϕ_2) of hybrid nanofluids is added to the different base fluids respectively. The radiative heat flux are [3,25]

$$q_r = -\frac{4\sigma^*}{3k^*}\frac{\partial T^4}{\partial y^*} , \qquad (13)$$

where σ^* is the Stefan-Boltzmann constant and k^* is the mean absorption coefficient. Therefore the equation (4) can be written as

$$(\rho C_p)_{hnf}\left(u^*\frac{\partial T}{\partial x^*} + v^*\frac{\partial T}{\partial y^*}\right) = k_{hnf}\frac{\partial^2 T}{\partial y^{*2}} + \frac{16\sigma^* T_\infty^3}{3k^*}\frac{\partial^2 T}{\partial y^{*2}} , \qquad (14)$$

The following transformations are [1]

$$x = \frac{x^*}{L}, \quad y = \frac{y^*}{L}Gr^{1/4}, \quad r = \frac{r^*}{L}, \quad u = \frac{u^*}{U} , \quad v = \frac{v^*}{U}Gr^{1/4}, \quad w = \frac{w^*}{\Omega L},$$

$$\Theta = \frac{T - T_0}{T_r - T_0} , \quad U = [g\cos\gamma\,(\beta_T)_f L(T_r - T_0)]^{\frac{1}{2}} , \quad r = x\sin\gamma \qquad (15)$$

where u*, v* and w* are the dimensional velocity components in the x*, y* and θ directions. The dimensionless equations (1) – (4) are given as

$$\frac{\partial}{\partial x}(ru) + \frac{\partial}{\partial y}(rv) = 0 , \qquad (16)$$

$$u\frac{\partial u}{\partial x}+v\frac{\partial u}{\partial y}-\frac{Re^2}{Gr}\frac{r'}{r}w^2 = \frac{1}{(1-\phi_2)\left[1-\phi_1+\phi_1\frac{\rho_{s_1}}{\rho_f}\right]+\phi_2\left(\frac{\rho_{s_2}}{\rho_f}\right)}\left\{\frac{1}{(1-\phi_1)^{2.5}(1-\phi_2)^{2.5}}\left(1+\frac{1}{\beta}\right)\frac{\partial^2 u}{\partial y^2} + \left[(1-\phi_2)\left[1-\phi_1+\phi_1\frac{(\rho\beta_T)_{s_1}}{(\rho\beta_T)_f}\right]+\phi_2\frac{(\rho\beta_T)_{s_2}}{(\rho\beta_T)_f}\right]\Theta-\frac{Da^{-1}u}{(1-\phi_1)^{2.5}(1-\phi_2)^{2.5}} - \frac{\sigma_{hnf}}{\sigma_f}M\Lambda^2 u\right\} \quad (17)$$

$$u\frac{\partial w}{\partial x}+v\frac{\partial w}{\partial y}+uw\frac{r'}{r} = \frac{1}{(1-\phi_2)\left[1-\phi_1+\phi_1\frac{\rho_{s_1}}{\rho_f}\right]+\phi_2\left(\frac{\rho_{s_2}}{\rho_f}\right)}\left\{\frac{1}{(1-\phi_1)^{2.5}(1-\phi_2)^{2.5}}\left(1+\frac{1}{\beta}\right)\frac{\partial^2 w}{\partial y^2}-\frac{Da^{-1}w}{(1-\phi_1)^{2.5}(1-\phi_2)^{2.5}}-\frac{\sigma_{hnf}}{\sigma_f}M\Lambda^2 w\right\} \quad (18)$$

$$u\frac{\partial \Theta}{\partial x}+v\frac{\partial \Theta}{\partial y}=\frac{1}{Pr}\frac{1}{(1-\phi_2)\left[1-\phi_1+\phi_1\frac{(\rho C_p)_{s1}}{(\rho C_p)_f}\right]+\phi_2\left(\frac{(\rho C_p)_{s2}}{(\rho C_p)_f}\right)}\left[\frac{k_{hnf}}{k_f}+R\right]\frac{\partial^2\Theta}{\partial y^2}, \quad (19)$$

The boundary conditions are transformed

$$u(x,0)=0,\quad v(x,0)=0,\quad w(x,0)=r,\quad \Theta(x,0)=x,$$
$$u = w = \Theta = 0 \;\; at \;\; y\to\infty. \quad (20)$$

A stream function ψ can be defined as:

$$ru=\frac{\partial\psi}{\partial y},\qquad rv=-\frac{\partial\psi}{\partial x}, \quad (21)$$

The boundary layer variables according to

$$\psi(x,y)=xrF(y),\qquad w=rG(y),\qquad \Theta=xH(y) \quad (22)$$

With the help of above transformations (22), the governing model becomes

$$\frac{\left(1+\frac{1}{\beta}\right)}{(1-\phi_1)^{2.5}(1-\phi_2)^{2.5}}F''' + \left[(1-\phi_2)\left[1-\phi_1+\phi_1\frac{\rho_{s_1}}{\rho_f}\right]+\phi_2\frac{\rho_{s_2}}{\rho_f}\right]\left[2FF''-F'^2+\varepsilon G^2\right] + \left[(1-\phi_2)\left[1-\phi_1+\phi_1\frac{(\rho\beta_T)_{s_1}}{(\rho\beta_T)_f}\right]+\phi_2\frac{(\rho\beta_T)_{s_2}}{(\rho\beta_T)_f}\right]H-\frac{Da^{-1}}{(1-\phi_1)^{2.5}(1-\phi_2)^{2.5}}F' - \frac{\sigma_{hnf}}{\sigma_f}M\Lambda^2F'=0, \quad (23)$$

$$\frac{1}{(1-\phi_1)^{2.5}(1-\phi_2)^{2.5}}\left(1+\frac{1}{\beta}\right)G'' + \left[(1-\phi_2)\left[1-\phi_1+\phi_1\frac{\rho_{s_1}}{\rho_f}\right]+\phi_2\frac{\rho_{s_2}}{\rho_f}\right]\left[2FG'-2F'G\right] - \frac{Da^{-1}}{(1-\phi_1)^{2.5}(1-\phi_2)^{2.5}}G-\frac{\sigma_{hnf}}{\sigma_f}M\Lambda^2G=0, \quad (24)$$

$$\left[\frac{k_{hnf}}{k_f} + R\right] H'' + 2Pr\left[(1-\phi_2)\left[1-\phi_1+\phi_1\frac{(\rho C_p)_{s_1}}{(\rho C_p)_f}\right] + \phi_2\left(\frac{(\rho C_p)_{s_2}}{(\rho C_p)_f}\right)\right]\left[FH' - \frac{1}{2}F'H\right] = 0, \quad (25)$$

where

$Re = \frac{\Omega L^2}{\nu_f}$ is a Reynolds number, $\Lambda = \frac{b(x)}{r\sqrt{1-r'^2}}$ is a magnetic field function,

$Gr = \left(\frac{UL}{\nu_f}\right)^2$ is a Grashof number, $Pr = \frac{\nu_f}{\alpha_f}$ is a Prandtl number,

$M = \frac{\sigma_f B_0^2 L}{U\rho_f}$ is a Magnetic parameter, $\varepsilon = \frac{(Resin\gamma)^2}{Gr}$ is a Spin parameter,

$Da = \frac{KU}{\nu_f L}$ is a Darcy number, $R = \frac{16\sigma^* T_\infty^3}{3k^* k_f}$ is a Radiation parameter,

$B = B_0 b(x)/(r\sqrt{1-r'^2})$ is a magnetic field strength

and

$$F = 0, \quad F' = 0, \quad G = 1, \quad H = 1 \ at \ y = 0,$$
$$F' \to 0, \quad G \to 0, \quad H \to 0 \quad as \ y \to \infty. \quad (26)$$

The physical quantities of engineering interest are surface drag coefficient C_f, and heat transfer rate Nu are

$$C_f = \frac{2r_w}{\rho_f U^2}, \quad Nu = \frac{Lq_w}{k_f(T_r - T_0)} \quad (27)$$

where r_w, q_w represents the shearing stress and surface heat flux respectively as,

$$r_w = \left(1+\frac{1}{\beta}\right)\mu_{hnf}\left(\frac{\partial u^*}{\partial y^*}\right)_{y^*=0}, \quad q_w = -k_{hnf}\left(\frac{\partial T}{\partial y^*}\right)_{y^*=0} + (q_r)_{y^*=0} \quad (28)$$

The non – dimensional form becomes,

$$C_f Gr^{\frac{1}{4}} = 2\left(1+\frac{1}{\beta}\right)\left(\frac{\mu_{hnf}}{\mu_f}\right) xF''(0), \quad NuGr^{-\frac{1}{4}} = -\left(\frac{k_{hnf}}{k_f} + R\right) xH'(0) \quad (29)$$

3. Solution Procedure

The Equation (23) – (25) confined to the boundary constraints (26) has been solved by fourth order Runge-Kutta scheme with shooting procedure. We indicate $F = y_1$, $G = y_4$, $H = y_6$ for our present model and illustrate a vital steps of the method are defined as:

$$y_1' = y_2$$
$$y_2' = y_3$$
$$y_3' = \left(1+\frac{1}{\beta}\right)^{-1}\left((1-\phi_1)^{2.5}(1-\phi_2)^{2.5}\right)\Big\{\frac{\sigma_{hnf}}{\sigma_f}M\Lambda^2 y_2 + \frac{Da^{-1}}{(1-\phi_1)^{2.5}(1-\phi_2)^{2.5}}y_2$$
$$-\left[(1-\phi_2)\left[1-\phi_1+\phi_1\frac{\rho_{s_1}}{\rho_f}\right]+\phi_2\frac{\rho_{s_2}}{\rho_f}\right]\left[2y_1y_3 - y_2^2 + \varepsilon y_4^2\right]$$
$$-\left[(1-\phi_2)\left[1-\phi_1+\phi_1\frac{(\rho\beta_T)_{s_1}}{(\rho\beta_T)_f}\right]+\phi_2\frac{(\rho\beta_T)_{s_2}}{(\rho\beta_T)_f}\right]\left[y_6\right]\Big\}$$

$$y_4' = y_5$$

$$y_5' = \left(1+\frac{1}{\beta}\right)^{-1} \left((1-\phi_1)^{2.5}(1-\phi_2)^{2.5}\right) \left[\frac{\sigma_{hnf}}{\sigma_f} M\Lambda^2 y_4 + \frac{Da^{-1}}{(1-\phi_1)^{2.5}(1-\phi_2)^{2.5}} y_4 - \left[(1-\phi_2)\left[1-\phi_1+\phi_1\frac{\rho_{s_1}}{\rho_f}\right]+\phi_2\frac{\rho_{s_2}}{\rho_f}\right]\left[2y_1 y_5 - 2y_2 y_4\right]\right]$$

$$y_6' = y_7$$

$$y_7' = -2Pr\ \left[(1-\phi_2)\left[1-\phi_1+\phi_1\frac{(\rho C_p)_{s_1}}{(\rho C_p)_f}\right]+\phi_2\left(\frac{(\rho C_p)_{s_2}}{(\rho C_p)_f}\right)\right]\left[\frac{k_f}{k_{hnf}}+\frac{1}{R}\right]\left[y_1 y_7 - \frac{1}{2} y_2 y_6\right] \tag{30}$$

and

$$y_1(0)=0, y_2(0)=0, y_4(0)=1, y_6(0)=1,$$
$$y_2(\infty)=0, y_4(\infty)=0, y_6(\infty)=0, \tag{31}$$

4. Results and Discussion

From this section, the hybrid Casson convective flow over a rotating cone along with magnetic field and thermal radiation with porous medium have been investigated. Here, we deal with three types of hybrid nanoparticles are $Al_2O_3 - TiO_2$, TiO_2 – Cu and Al_2O_3 – Cu with water and sodium alginate as the base fluids and also examine that in the case of Newtonian base fluid appear though $\beta \rightarrow \infty$. The flow behavior of some pertinent parameters are shown graphically and the physical quantities are analyzed through table. Some of the fixed values are $M = \varepsilon = R = \Lambda = 1,\ Da = 0.1,\ \beta = 1, Pr = 6.2$(Water)$, Pr = 6.5$ (Sodium Alginate), until they are particularly specified.

Figs.2 (a-c) – 4 (a-c) are monitored to examine the physical characteristics of tangential velocity, swirl velocity and thermal profile for various values of M in three hybrid nanofluids. The growing M reduces both tangential velocity (Fig.2 (a-c)) and swirl velocity (Fig.3 (a-c)) because Lorentz force produce more resistance to the transport development and decreases viscous frontier consistency. At the same time, Newtonian base fluid is greater than non-Newtonian base fluid in tangential velocity (Fig.2 (a-c)) by the cause of Newtonian base fluid acceleration is higher in three hybrid nanoparticles. But in swirl velocity (Fig.3 (a-c)), it is controversy while increasing the values of M in three hybrid nanoparticles. Therefore, we conclude that base fluids have opposite reaction in tangential velocity and swirl velocity profile. Fig.4 (a-c) exhibit the temperature profile for three hybrid nanofluids. From this plot, it is seen that the heat range is direct proportion to M. Due to the nature, hybrid nanofluid particles are act as energy carrying fluid, this causing increase in thermal profile. Moreover, it is noticed in the base fluids that the flow of fluid is hiking more for sodium alginate based hybrid nanofluid as its kinematic viscosity has enhanced in $Al_2O_3 - TiO_2$, TiO_2 – Cu and Al_2O_3 – Cu hybrid nanoparticles.

Figs.5 (a-c) – 7 (a-c) are prepared to analyze the impact of Spin parameter ε on tangential velocity, swirl velocity and heat flow in hybrid nanofluids respectively. Fig.5 (a-c) exhibit that a rise in the ε expanding the acceleration and also shows miscellaneous behavior when Coriolis effects created spinning. However, in swirl velocity profile (Fig.6 (a-c)), there is a dwindled from the wall to the free flow. Comparing the base fluids in $Al_2O_3 – TiO_2$, $TiO_2 – Cu$ and $Al_2O_3 – Cu$ hybrid nanoparticles, water based hybrid nanofluid is intensified in tangential velocity (Fig.5 (a-c)) because its density is higher and in swirl velocity (Fig.6 (a-c)), converse manner is notified for all the three hybrid nanoparticles. In Fig.7 (a-c), the changes in temperature profile of hybrid nanofluid for various estimates of ε are elucidated. The temperature is inversely proportional to the spin parameter ε. Since the thermal boundary layer thickness has been declined. While analyzing the base fluids in three hybrid nanoparticles, water based hybrid nanofluid has deteriorated and its thermal diffusivity also dropped off in Fig.7 (a-c).

Figs.8 (a-c) – 10 (a-c) depicts the influence of Darcy number Da on tangential velocity, swirl velocity and temperature profile in three hybrid nanofluids. We currently see that the Figs.8 (a-c) and 9 (a-c) shows the fluctuation of F' and G for swelling values of Da. The curve reflects that as we upsurging the values of Da, the porosity of the medium also gets escalated. Hence, the fluid flow hikes in twain velocity profiles (tangential, swirl). As we observed base fluids in tangential velocity and swirl velocity profile, it clearly shows that Newtonian base fluid is increased in tangential velocity and has the opposite trend is the outcome for swirl velocity in Fig.8 (a-c). Because electrical conductivity of Newtonian base fluid has more strengthened than non-Newtonian base fluid for all the three hybrid nanoparticles. Characteristics of Da on H is evaluated in Fig.10 (a-c). It is perceived that greater values of Da are found to fairly depreciate the thermal flow for all the hybrid nanofluids. Whereas in base fluids, sodium alginate based hybrid nanofluid has greater velocity and its boundary layer gets thickened in temperature profile, while amplifying the values of Da for all the three hybrid nanoparticles.

Figs.11 (a-c) – 13 (a-c) exemplify the performance of R on tangential momentum, swirl momentum and thermal profile in three hybrid nanofluids respectively. It is observed from Fig.11 (a-c), that F' is strongly intensified with an increment of R. The velocity flow ascends quickly near cone surface and then dropped evenly in the free stream for all the three hybrid nanofluids. In addition, water based hybrid nanofluid is expanded in tangential velocity (Fig.11 (a-c)) as its specific heat is improved for all the three hybrid nanoparticles. The swirl velocity profile G is analyzed in Fig.12 (a-c) which reports the range of R in three hybrid nanofluids. The momentum boundary layer thickness has been diminished by an increment of R. This is similar for all the three hybrid nanofluids in Fig.12 (a-c). Additionally, non-Newtonian base fluid is upturned as its denseness is lower for all the three hybrid nanoparticles. Fig.13 (a-c) exposes the nature of R on temperature profile H. The leading assign values of R elevates the thermal frontier consistency. Because it extracts the energy through the fluid in movement, which ultimately uplifted a profile. While considering the two base fluids in three hybrid nanoparticles, non-Newtonian base fluid has enlarged due to the fact that Prandtl number of non-Newtonian base fluid is enhanced.

Figs.14 (a-c) – 16 (a-c) illustrates the action of variation in Casson parameter β on two momentum profiles and heat flow profile in three hybrid nanofluids respectively. The momentum boundary layer thickness has been amplified in tangential velocity profile (Fig.14 (a-c)). Therefore, the velocity will be expanded with the expansion of β. Fig.15 (a-c) illustrates the change of velocity in swirl velocity profile. The raise in β is used to diminish the yield stress of the fluid flow. Due to this fact, we have seen a notable deceleration in Fig.15 (a-c). The temperature curve in Fig.16 (a-c) dependent upon the Casson parameter, which prompts the shrinkage of thermal boundary layer thickness. Consequently, the temperature profile will be reduced in three hybrid nanofluids.

Table 2 displays a validation of the current results with Beg [1] and Ece [26] and we terminate that the outcomes are excellent in a good manner.

Tables 3 and 4 are presented the numerical range of surface drag force and heat transfer rate against pertinent variables for $Al_2O_3 – TiO_2$, $TiO_2 – Cu$ and $Al_2O_3 – Cu$ hybrid nanoparticles with Newtonian and non-Newtonian base fluids. The surface drag force augments with larger ε, Da, R and has opposite manner while increasing the range of M and β in Table 2 for three hybrid nanofluids. The Skin friction coefficient values of non-Newtonian base fluid has greater velocity than Newtonian base fluid. Additionally, the Nusselt number in Table 3 is superior for ε, Da, R, β and also water based hybrid nanofluid's heat transfer rate is hiked. From Tables 2 and 3, we concluded that $TiO_2 – Cu$ and $Al_2O_3 – Cu$ hybrid nanoparticles are larger than $Al_2O_3 – TiO_2$ hybrid nanoparticles.

5. Conclusion

Hybrid MHD Casson nanofluid stream with thermal radiation through spinning cone with permeable media is investigated by considering $Al_2O_3 – TiO_2$, $TiO_2 – Cu$ and $Al_2O_3 – Cu$ as hybrid nanoparticles with twain distinct base fluids. The main points of the study are discussed below:

- Elevating the values of M, the velocity distribution (tangential, swirl), surface drag force coefficient and heat transfer rate are diminished in all the three hybrid nanofluids.
- The Spin parameter ε enhances the tangential velocity and shows a converse effect on the swirl velocity.
- While intensifying the Radiation parameter, the temperature as well as heat transfer will also be hiked for all the hybrid nanofluids.
- The velocity profiles, the Skin friction coefficient and local Nusselt number are upsurged with mounting Da for all the hybrid nanofluids.
- The Casson parameter decelerates the skin friction coefficient for non-Newtonian base fluid in three hybrid nanoparticles.
- Newtonian base fluid is increasing for Da and R for both skin friction coefficient and Nusselt number in three hybrid nanoparticles.

Table 2

Validation results for F''(0) and -H'(0) with Beg [1] and Ece [26], when ϕ =0.

Pr	ε	F''(0)			-H'(0)		
		Maple 17 Beg [1]	Ece [26]	Present Study	Maple 17 Beg [1]	Ece [26]	Present Study
1	0	0.68148	0.68150	0.67494	0.63885	0.63886	0.63560
	0.5	0.84648	0.84650	0.84117	0.67193	0.67194	0.66951
	1.0	1.00194	1.00196	0.99745	0.70052	0.70053	0.69863
	2.0	1.29228	1.29230	1.28885	0.74868	0.74869	0.74745
10	0	0.42918	0.43327	0.43054	1.26598	1.27552	1.26850
	0.5	0.62280	0.62601	0.62102	1.54763	1.47165	1.46317
	1.0	0.79841	0.79828	0.79353	1.20756	1.60768	1.60107
	2.0	1.10990	1.10990	1.10598	1.80574	1.80575	1.80149

Table 3

Numerical range of Skin friction coefficient for H_2O and $NaC_6H_9O_7$ base fluids with different hybrid nanoparticles for dissimilar physical variables.

M	ε	Da	R	β	Al_2O_3 - TiO_2		TiO_2 - Cu		Al_2O_3 - Cu	
					H_2O	$NaC_6H_9O_7$	H_2O	$NaC_6H_9O_7$	H_2O	$NaC_6H_9O_7$
1	1	0.1	1	1	0.66677	0.88909	0.68424	0.90985	0.68392	0.90945
3					0.62772	0.84088	0.64400	0.86017	0.64371	0.85980
5					0.59505	0.80025	0.61036	0.81833	0.61009	0.81799
1	1	0.1	1	1	0.66677	0.88909	0.68424	0.90985	0.68392	0.90945
	2				0.87374	1.17794	0.90519	1.21843	0.90460	1.21765
	3				1.08054	1.46685	1.12596	1.52709	1.12511	1.52593
1	1	0.1	1	1	0.66677	0.88909	0.68424	0.90985	0.68392	0.90945
		0.9			1.07911	1.39676	1.11205	1.43837	1.11147	1.43761
		1.7			1.15017	1.48929	1.18656	1.53601	1.18593	1.53518
1	1	0.1	1	1	0.66677	0.88909	0.68424	0.90985	0.68392	0.90945
			1.5		0.67531	0.90283	0.69294	0.92375	0.69262	0.92335
			2		0.68011	0.91060	0.69782	0.93162	0.69750	0.93122
1	1	0.1	1	0.5	-	1.05068	-	1.07583	-	1.07534
				1	-	0.88909	-	0.90985	-	0.90945
				1.5	-	0.82395	-	0.84299	-	0.84263

Table 4

Numerical range of Nusselt number for H_2O and $NaC_6H_9O_7$ base fluids with different hybrid nanoparticles for dissimilar physical variables

M	ε	Da	R	β	Al_2O_3 - TiO_2		TiO_2 - Cu		Al_2O_3 - Cu	
					H_2O	$NaC_6H_9O_7$	H_2O	$NaC_6H_9O_7$	H_2O	$NaC_6H_9O_7$
1	1	0.1	1	1	1.82149	1.72336	1.83939	1.73857	1.83929	1.73849
3					1.73040	1.64580	1.74688	1.65956	1.74681	1.65950
5					1.65266	1.57909	1.66801	1.59169	1.66794	1.59165
1	1	0.1	1	1	1.82149	1.72336	1.83939	1.73857	1.83929	1.73849
	2				1.92627	1.84866	1.95119	1.87246	1.95099	1.87224
	3				2.02990	1.97145	2.06169	2.00345	2.06137	2.00310
1	1	0.1	1	1	1.82149	1.72336	1.83939	1.73857	1.83929	1.73849
		0.9			2.67018	2.44000	2.70713	2.47498	2.70682	2.47466
		1.7			2.79646	2.55039	2.83733	2.58938	2.83699	2.58902
1	1	0.1	1	1	1.82149	1.72336	1.83939	1.73857	1.83929	1.73849
			1.5		2.10426	1.99694	2.12216	2.01170	2.12206	2.01162
			2		2.41077	2.29187	2.42917	2.30667	2.42907	2.30658
1	1	0.1	1	0.5	-	1.64317	-	1.65872	-	1.65863
				1	-	1.72336	-	1.73857	-	1.73849
				1.5	-	1.75873	-	1.77376	-	1.77370

References

[1] O. A. Beg, M. J. Uddin, T. Beg, R. R. Gorla, Numerical simulation of self-similar thermal convection from a spinning cone in anisotropic porous medium, J. Hydrodynamics 28 (2) (2016) 184 – 194.

[2] P. Sambath, B. Pullepu, T. Hussain, S. A. Shehzad, Radiated chemical reaction impacts on natural convective MHD mass transfer flow induced by a vertical cone, Res. Phy. 8 (2018) 304 – 315.

[3] G. Makanda, P. Sibanda, Numerical analysis of free convection Casson fluid flow from a spinning cone in non-Darcy porous medium with partial slip and viscous dissipation effects, Int. J. Math. Comput. Meth. 1 (2016).

[4] B. Mallikarjuna, A. M. Rashad, A. K. Hussein, S. H. Raju, Transpiration and thermophoresis effects on non-Darcy convective flow past a rotating cone with thermal radiation, Arab. J. Sci. Eng. (2016).

[5] T. Hayat, B. Ahmed, F. M. Abbasi, A. Alsaedi, Peristaltic radiative flow of Sisko nanomaterial with entropy generation and modified Darcy's law, J. Therm. Anal. Calorim. (2020).

[6] A. B. M. Mohana Raju, G. S. S. Raju, B. Mallikarjuna, Unsteady nonlinear convective Darcy flow of a non – Newtonian fluid over a rotating vertical cone, IOP Conf. Series: Mat. Sci. Eng. 263 (2017) 062001.

[7] A. B. M. Mohana Raju, B. Mallikarjuna, Effects of nonlinear convection and variable properties on Darcy flow of non – Newtonian fluid over a rotating cone, Int. J. Res. Eng. Appl. Management 4 (2) (2018).

[8] N. Vedavathi, G. Dharmaiah, K. Venkatadri, S. A. Gaffar, Numerical study of radiative non-Darcy nanofluid flow over a stretching sheet with a convective Nield conditions and energy activation, Nonlinear Eng. 10 (2021) 159 – 176.

[9] B. K. Siddiqui, S. Batool, M.Y. Malik, Q.M. Hassan, A.S. Alqahtani, Darcy Forchheimer bioconvection flow of Casson nanofluid due to a rotating and stretching disk together with thermal radiation and entropy generation, Case Studies Therm. Eng. (2021).

[10] Y. Q. Song, S. A. Khan, M. Imran, H. Waqas, S. U. Khan, M. Ijaz Khan, S. Qayyum, Y. M. Chu, Applications of modified Darcy law and nonlinear thermal radiation in bioconvection flow of micropolar nanofluid over an off centered rotating disk, Alexandria Eng. J.60 (2021) 4607 – 4618.

[11] M. B. B. Hamida, K. Charrad, Natural convection heat transfer in an enclosure filled with an Ethylene Glycol – Copper nanofluid under magnetic fields,Numer. Heat Transf. 67 (2015) 902–920.

[12] A. K. Abdul Hakeem, B. Ganga, Convective heat transfer of nanofluid over an inclined stretching sheet in the presence of thermal radiation, Int. Conf. Math. Sci. (2014).

[13] B. Ganga, M. Govindaraju, A. K. Abdul Hakeem, Effects of inclined magnetic field on entropy generation in nanofluid over a stretching sheet with partial slip and nonlinear thermal radiation, Iran J. Sci. Technol. Transf. Mech. Eng. (2018).

[14] F. A. Alwawi, H.T. Alkasasbeh, A.M. Rashad and R. Idris, Natural convection flow of Sodium Alginate based Casson nanofluid about a solid sphere in the presence of a magnetic field with constant surface heat flux, J. Phy.: Conf. Series 1366 (2019) 012005.
[15] P. Ragupathi, A. K. Abdul Hakeem, S. Saranya, B. Ganga, Non – Darcian three-dimensional flow of Fe_3O_4/Al_2O_3 nanoparticles with $H_2O/NaC_6H_9O_7$ base fluids past a Riga plate embedded in a porous medium, Eur. Phys. J. Special Topics 228 (2019) 2571 – 2600.
[16] U. Khan, S. Bilal, A. Zaib, O. D. Makinde, A. Wakif, Numerical simulation of a nonlinear coupled differential system describing a convective flow of Casson gold–blood nanofluid through a stretched rotating rigid disk in the presence of Lorentz forces and nonlinear thermal radiation, Numer. Meth. Partial Diff. Eq. (2020) 1–21.
[17] C.S.K. Raju, S.U. Mamatha, P. Rajadurai, I. Khan, Nonlinear mixed thermal convective flow over a rotating disk in suspension of magnesium oxide nanoparticles with water and EG, Eur. Phys. J. Plus (2019) 134:196.
[18] A. Jamaludin, K. Naganthran, R. Nazar, I. Pop, MHD mixed convection stagnation-point flow of Cu-Al_2O_3/water hybrid nanofluid over a permeable stretching/shrinking surface with heat source/sink, Eur. J. Mech.B Fluids 84 (2020) 71–80.
[19] A. Hussanan, M. Qasim, Z. M. Chen, Heat transfer enhancement in sodium alginate based magnetic and non-magnetic nanoparticles mixture hybrid nanofluid, Physica A 550 (2020) 123957.
[20] T.A. Yusuf, F. Mabood, W.A. Khan, J.A. Gbadeyan, Irreversibility analysis of Cu-TiO_2-H_2O hybrid-nanofluid impinging on a 3-D stretching sheet in a porous medium with nonlinear radiation: Darcy-Forchhiemer's model, Alexandria Eng. J. (2020).
[21] Kh. Hosseinzadeh, A. Asadi, A. R. Mogharrebi, M. E. Azari, D. D. Ganji, Investigation of mixture fluid suspended by hybrid nanoparticles over vertical cylinder by considering shape factor effect, J. Therm. Anal. Calorim. (2020).
[22] H. Hanif, I. Khan S. Shafe, Heat transfer exaggeration and entropy analysis in magneto-hybrid nanofluid flow over a vertical cone: a numerical study, J. Therm. Anal. Calorim. (2020).
[23] S. Reddy, P. Sreedevi, A. J. Chamkha, Maxwell hybrid nanoliquid flow over vertical cone with Cattaneo – Christovheat flux and convective boundary condition, Authorea, (2020).
[24] I. Tlili, N. Sandeep, M. Girinath Reddy, H. A. Nabwey, Effect of radiation on engine oil-TC4/NiCr mixture nanofluid flow over a revolving cone in mutable permeable medium, Ain Shams Eng. J. (2020).
[25] E.N. Maraj, Z. Iqbal, E. Azhar, Z. Mehmood, A comprehensive shape factor analysis using transportation of MoS_2 – SiO_2 /H_2O inside an isothermal semi vertical inverted cone with porous boundary, Res. Phy. 8 (2018) 633 – 641.
[26] M.C. Ece, Free convection flow about a vertical spinning cone under a magnetic field, App. Math. Comput. 179 (2006) 231 – 242.

(a)

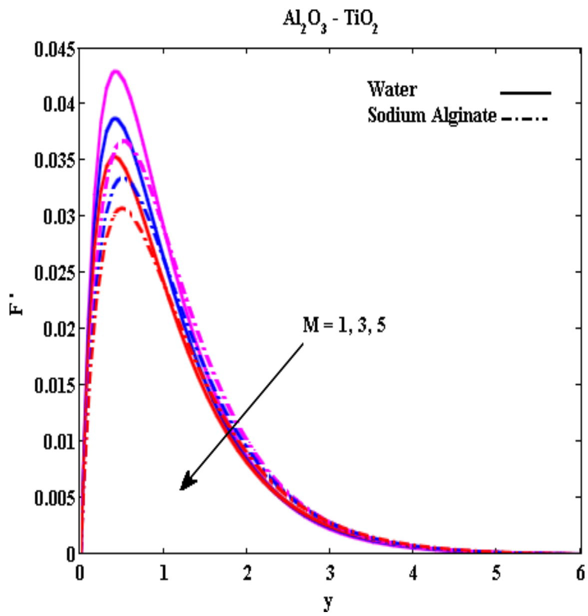

(b)

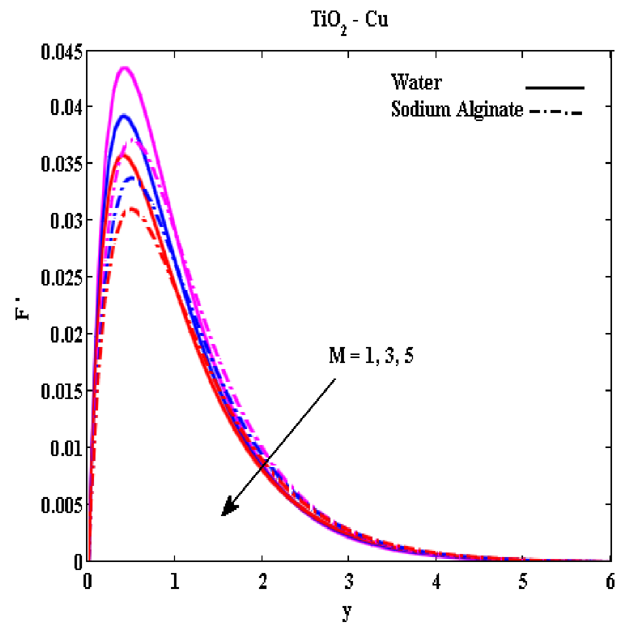

(c)

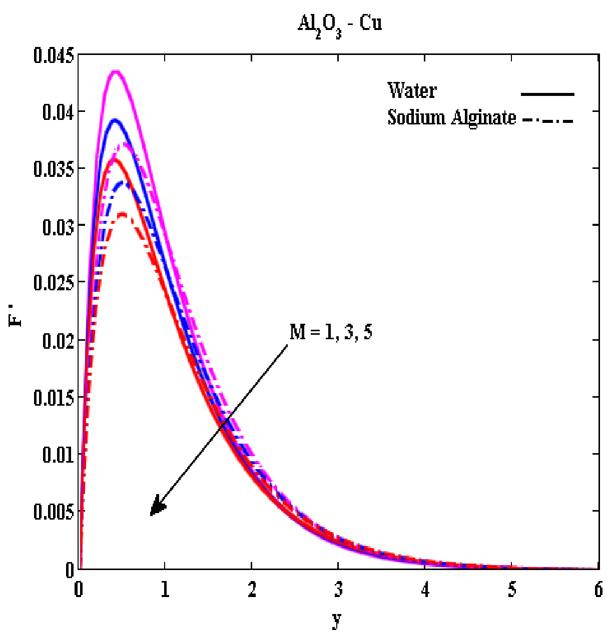

Fig.2 (a-c) Variation of M on F’

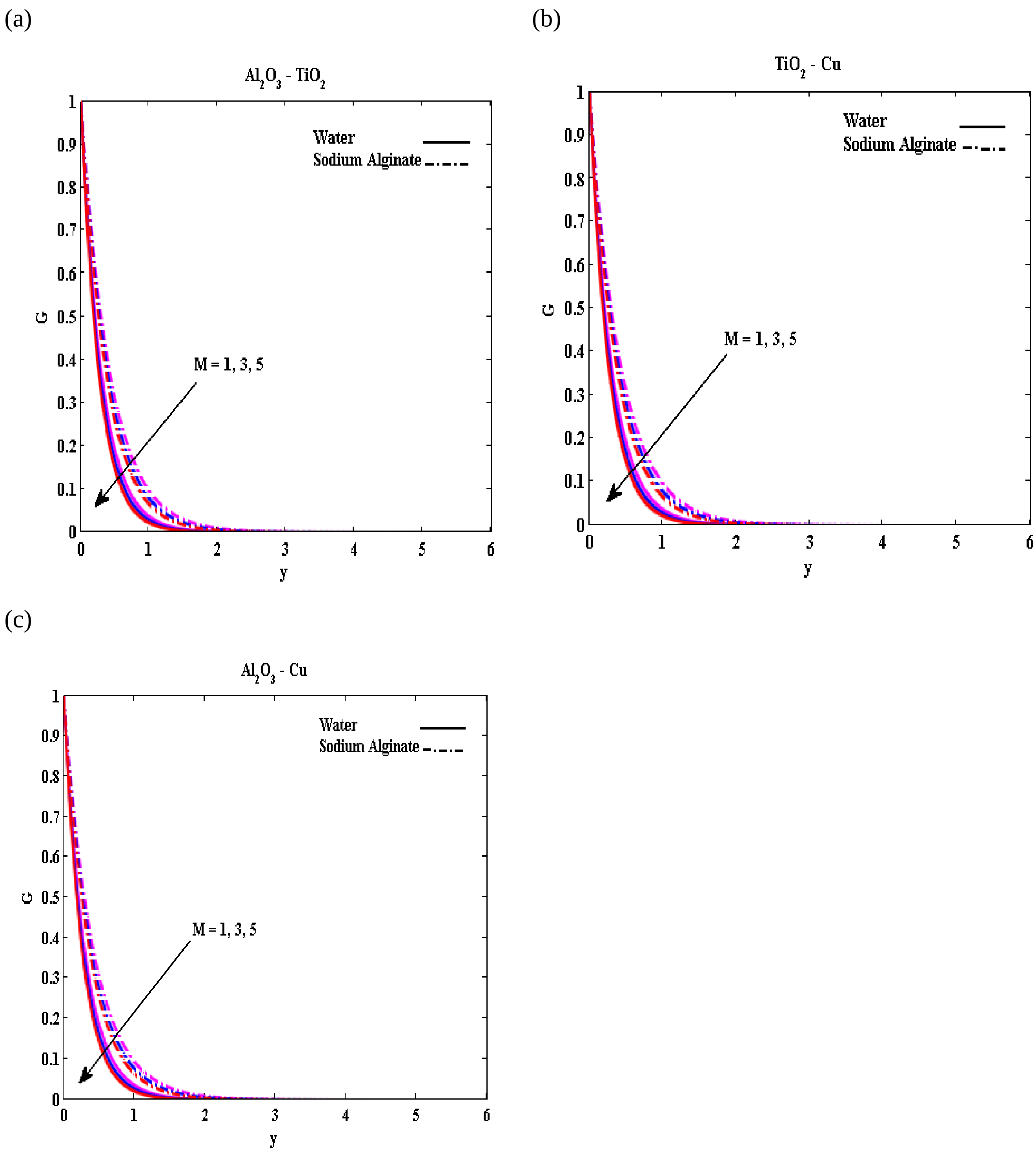

Fig.3 (a-c) Variation of M on G

(a)

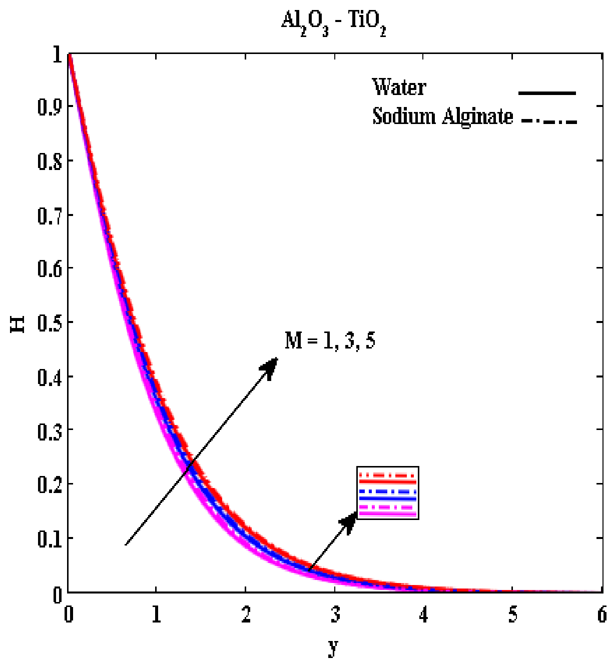

(b)

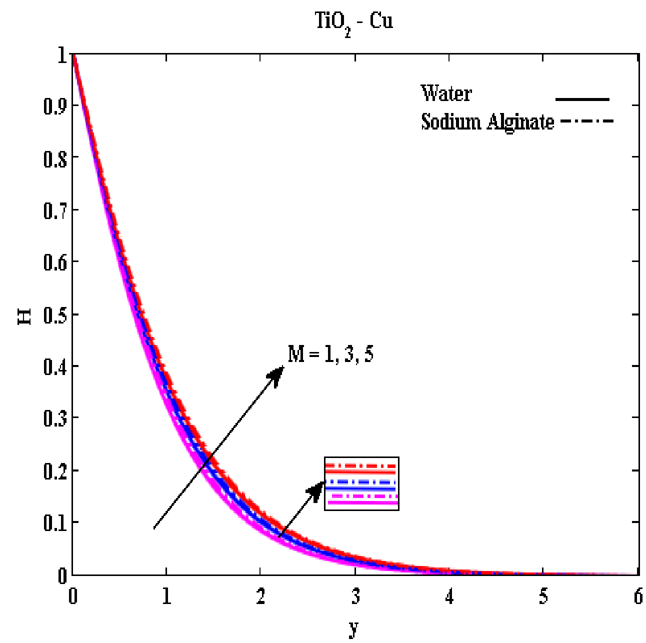

(c)

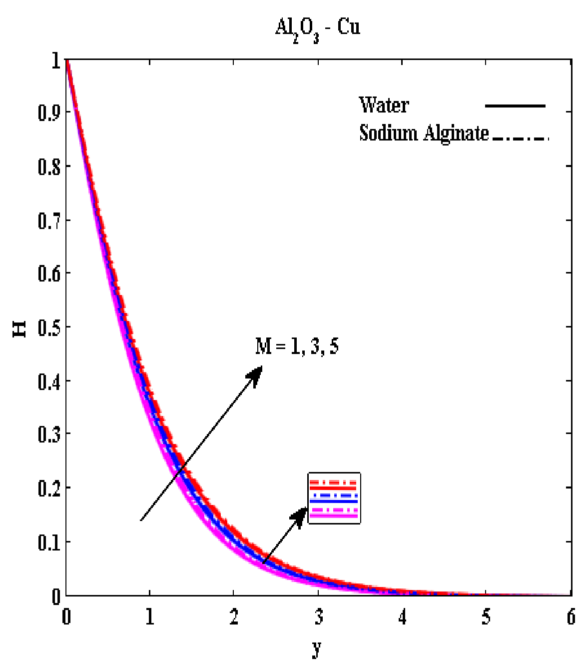

Fig.4 (a-c) Variation of M on H

(a)

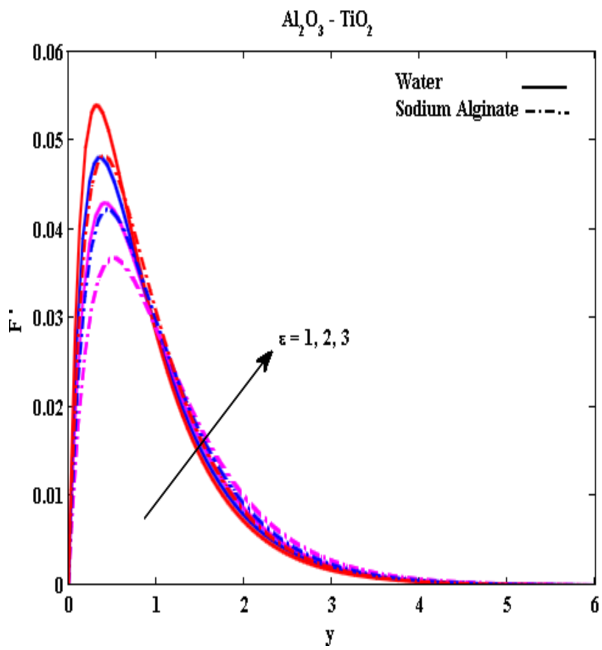

(b)

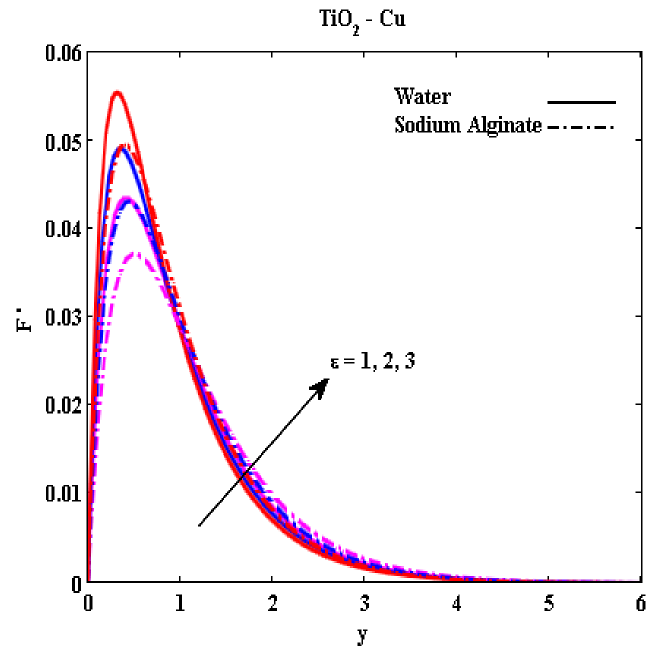

(c)

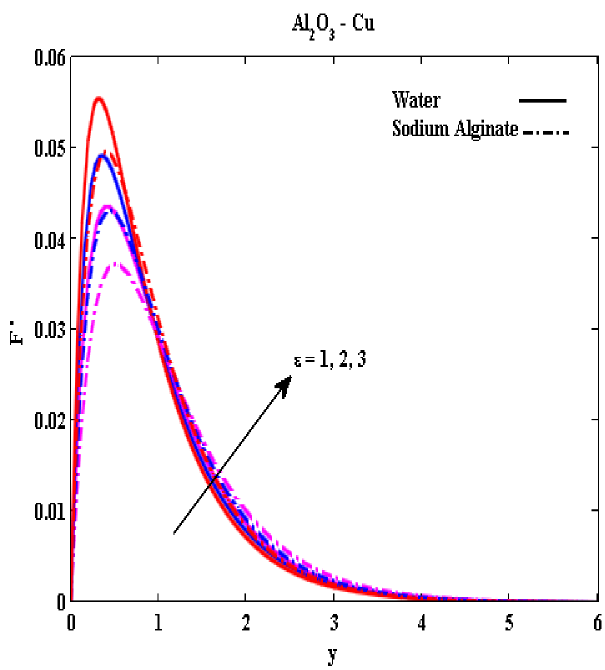

Fig.5 (a-c) Variation of ε on F’

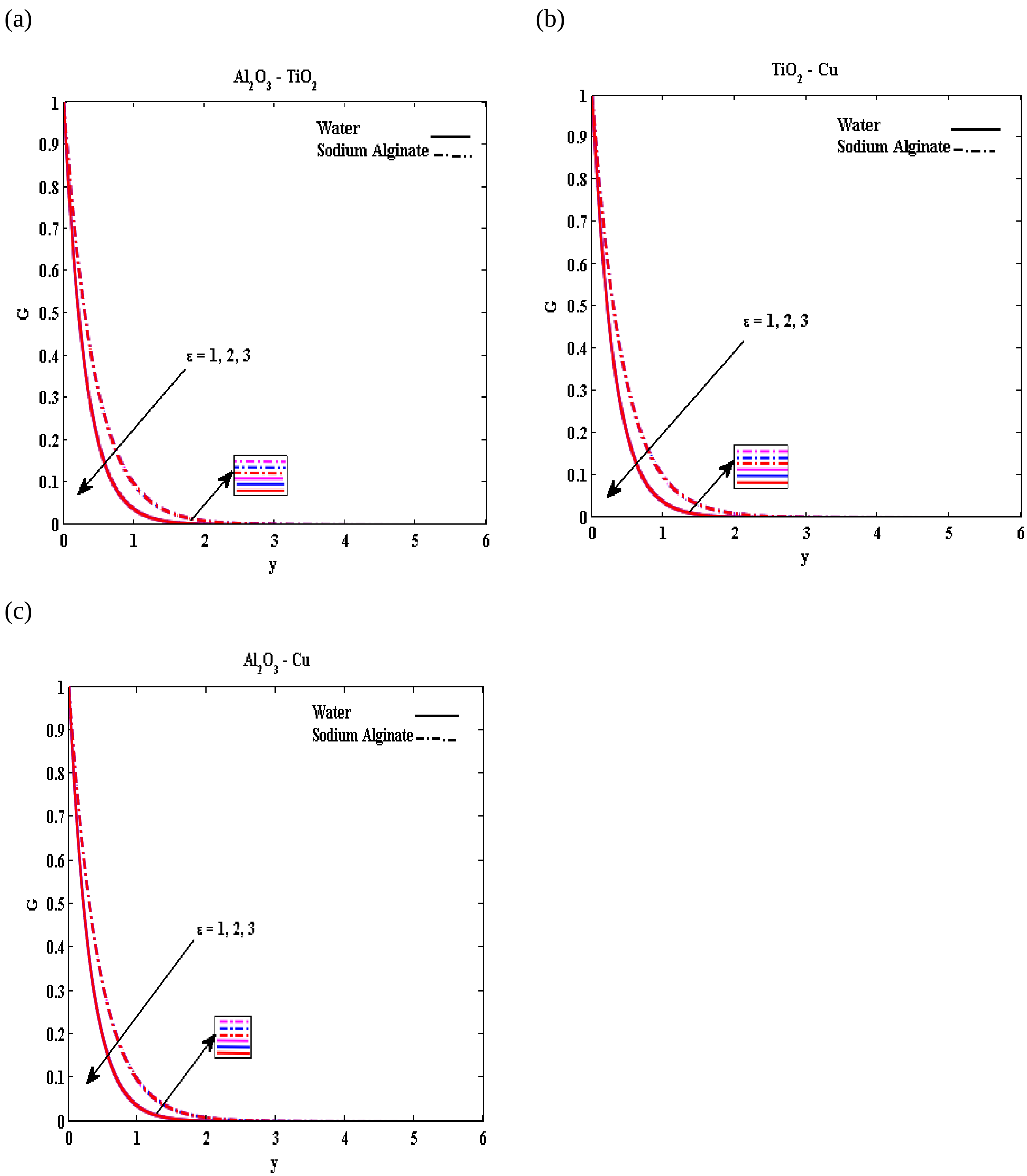

Fig.6 (a-c) Variation of ε on G

(a)

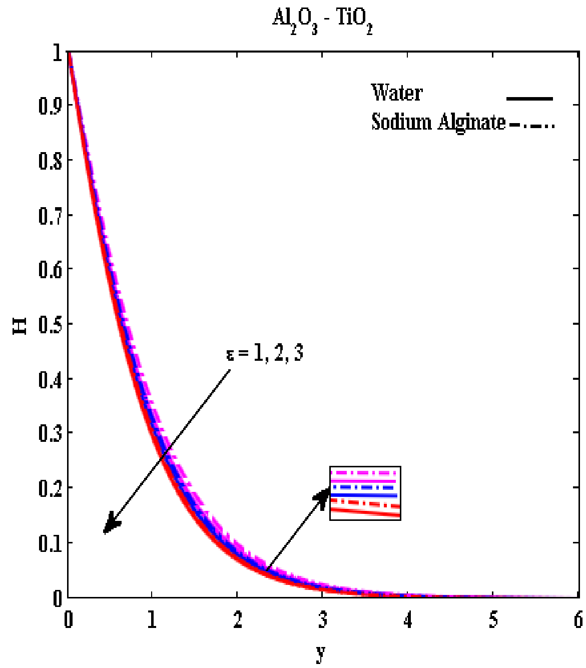

(b)

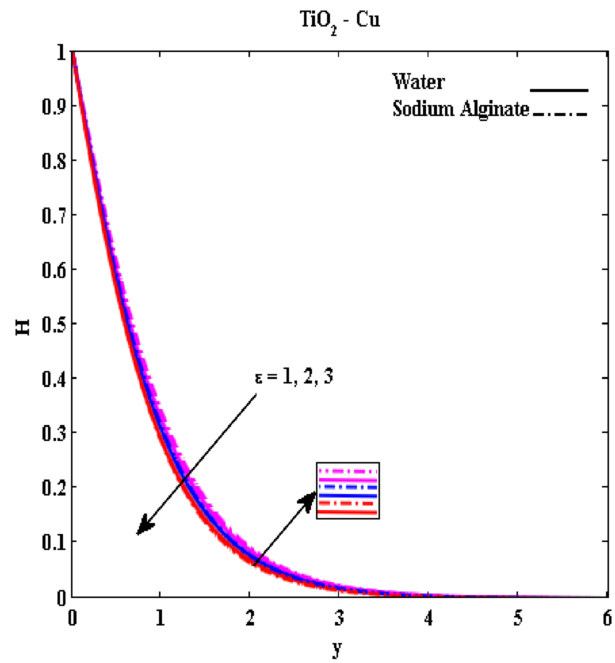

(c)

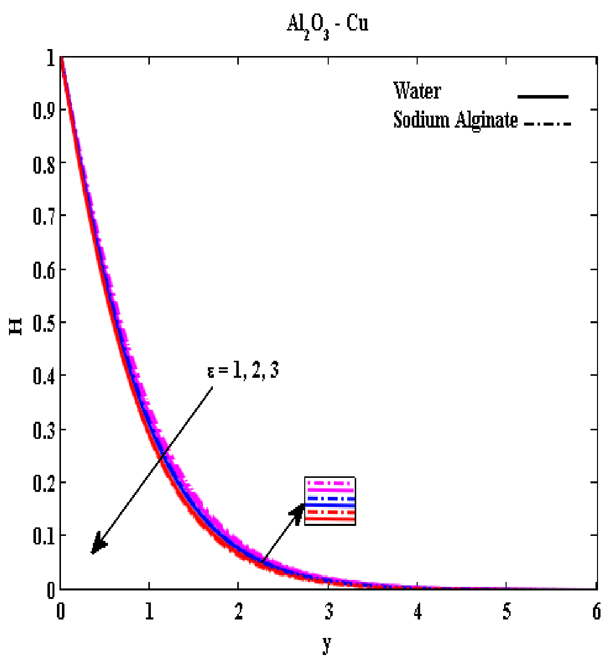

Fig.7 (a-c) Variation of ε on H

(a)

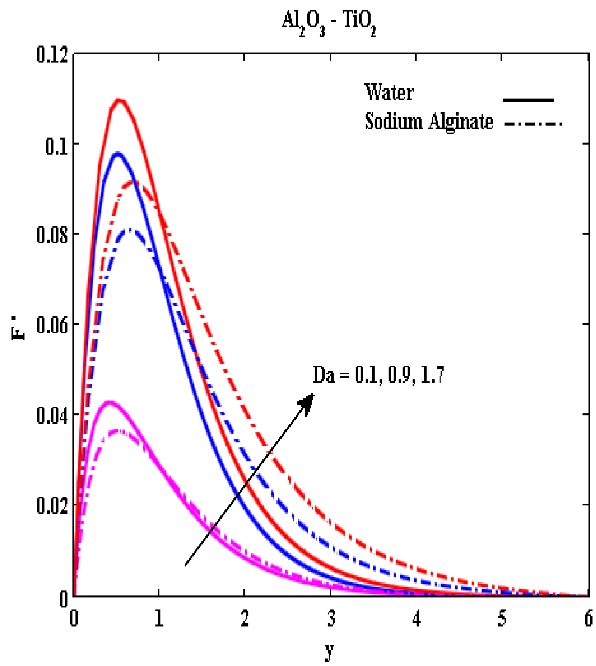

(b)

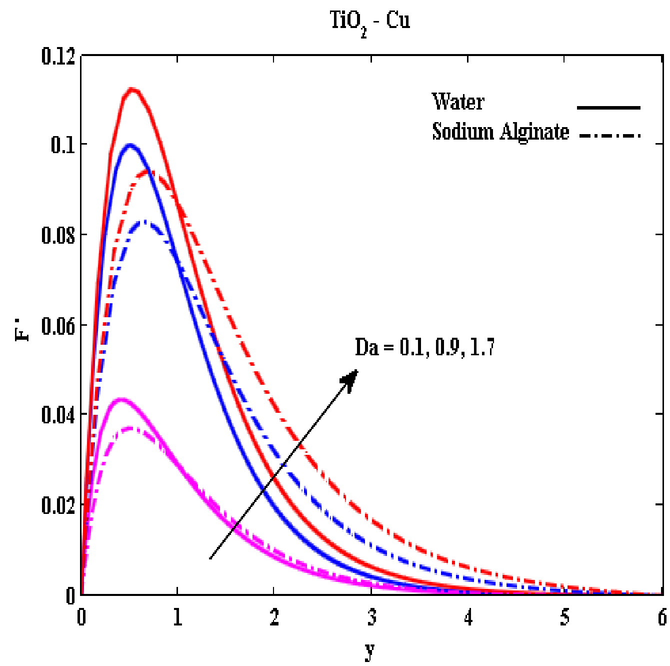

(c)

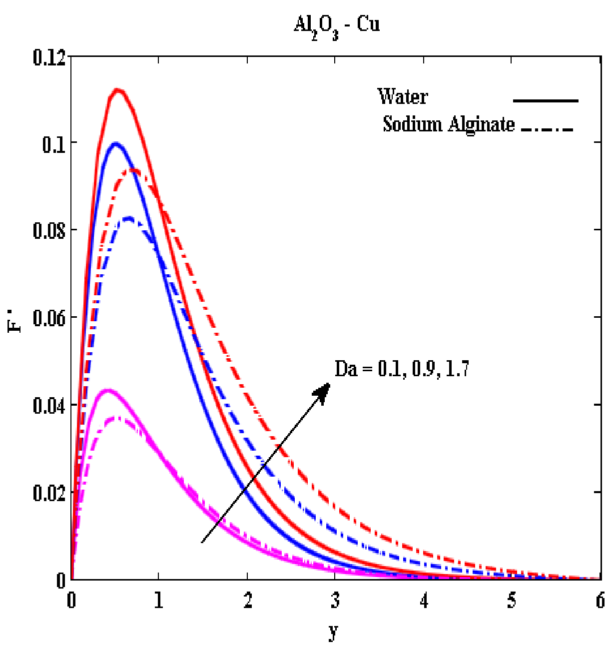

Fig.8 (a-c) Variation of Da on F’

(a)

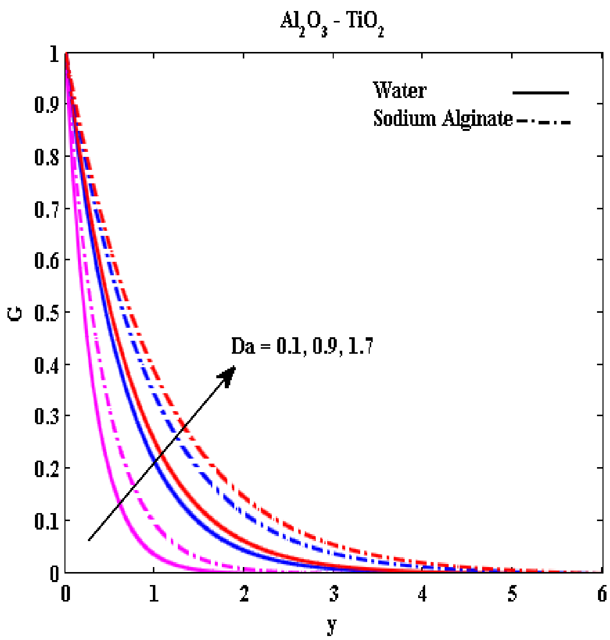

(b)

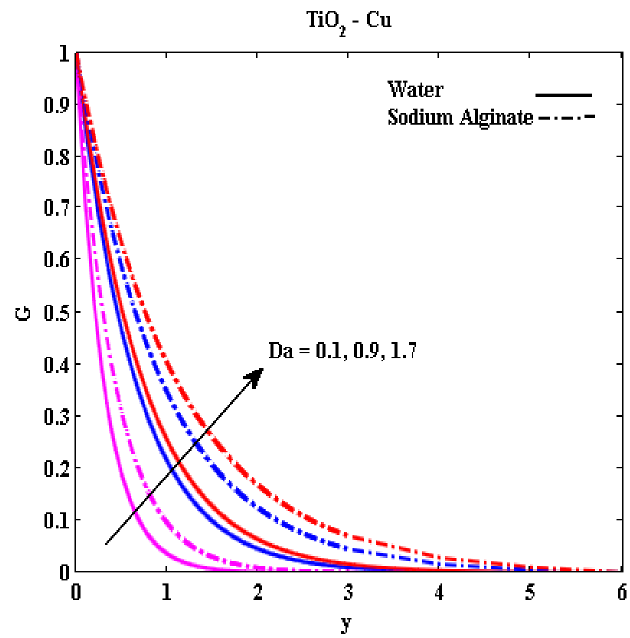

(c)

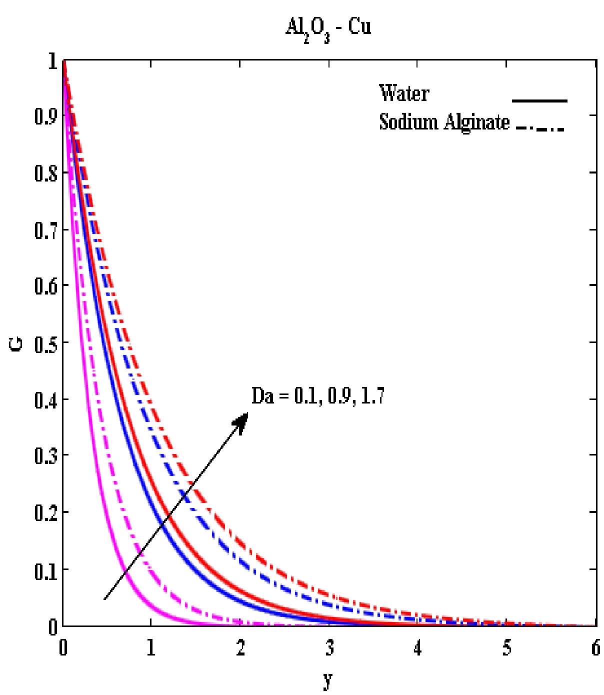

Fig.9 (a-c) Variation of Da on G

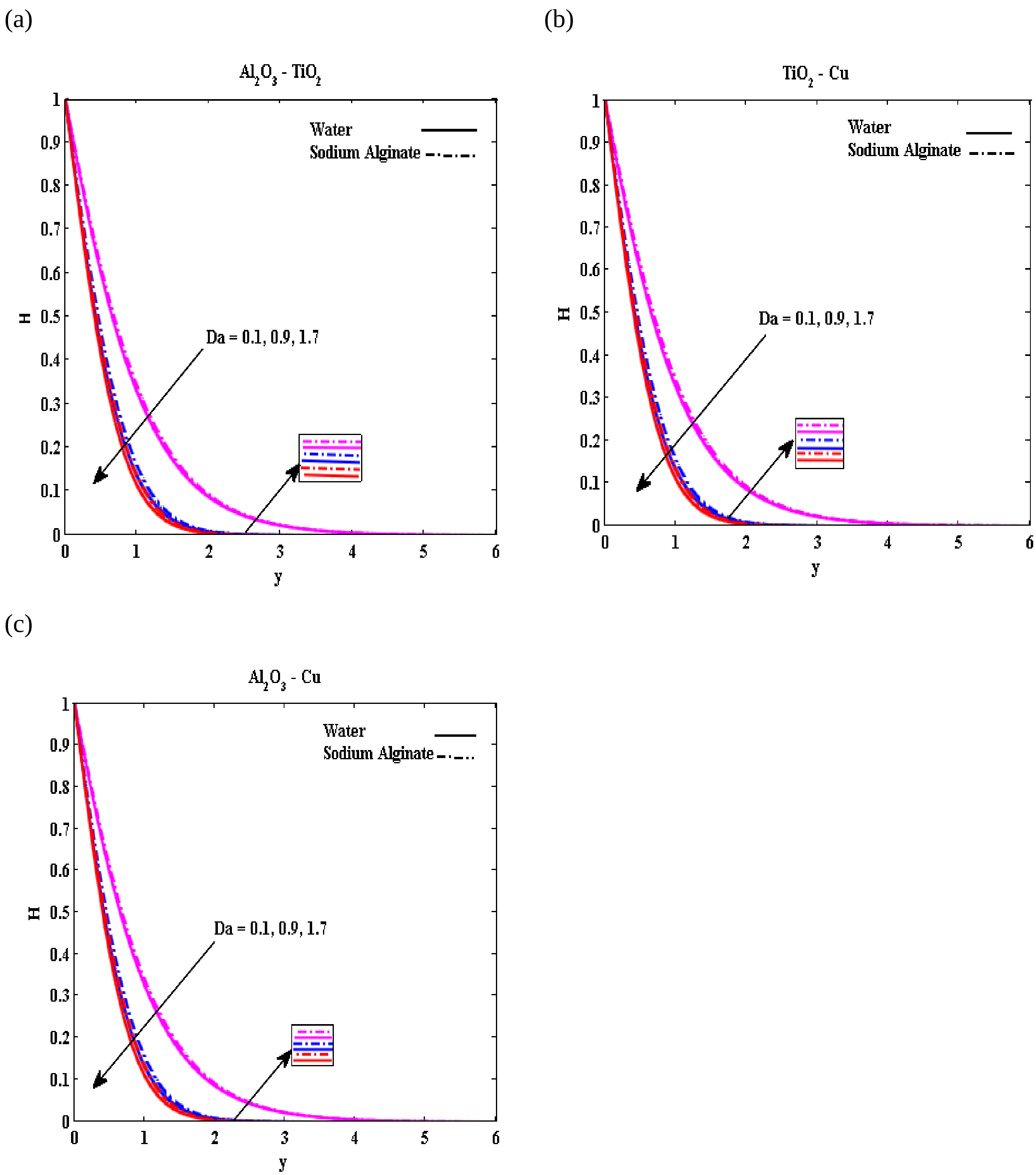

Fig.10 (a-c) Variation of Da on H

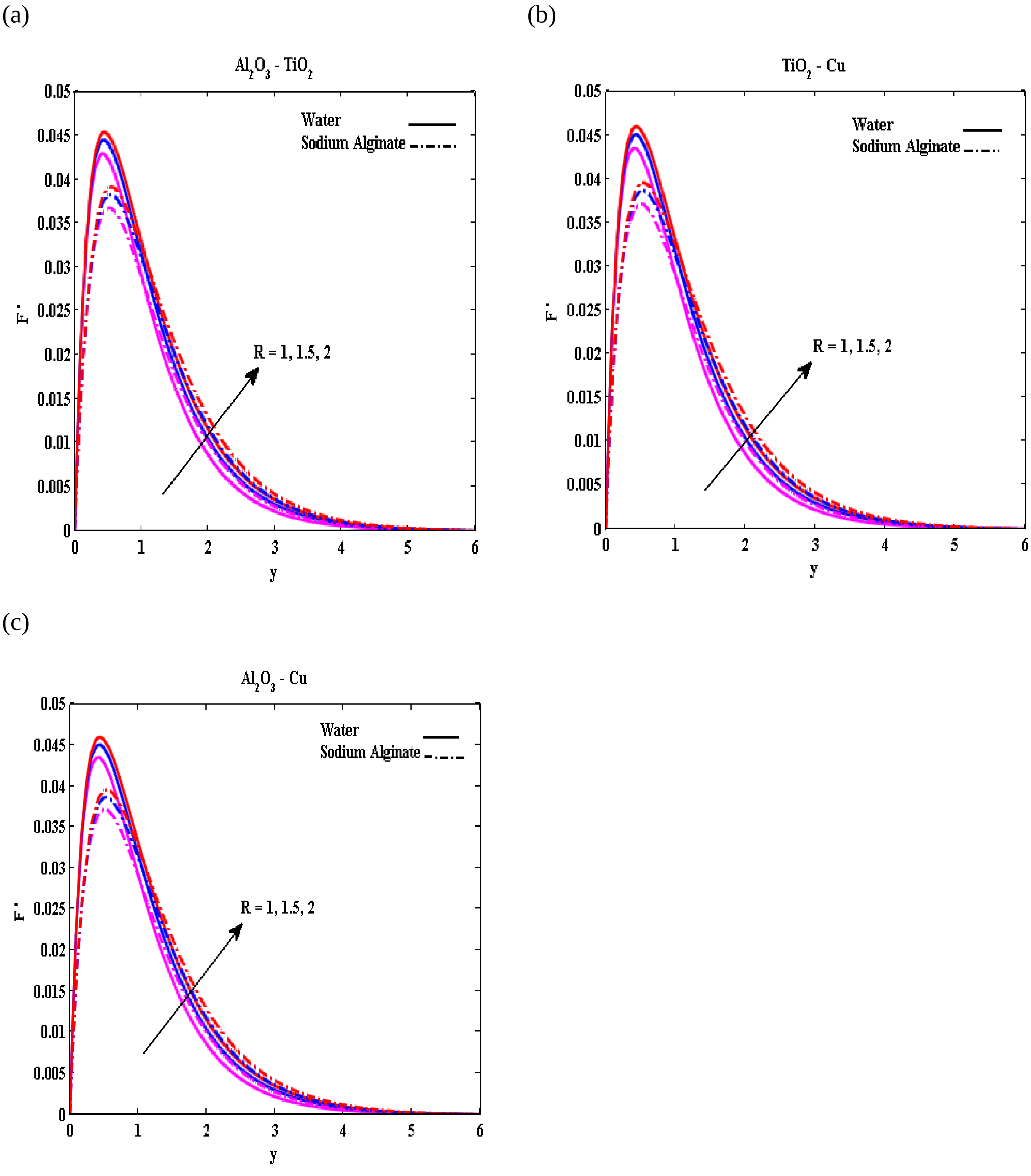

Fig.11 (a-c) Variation of R on F'

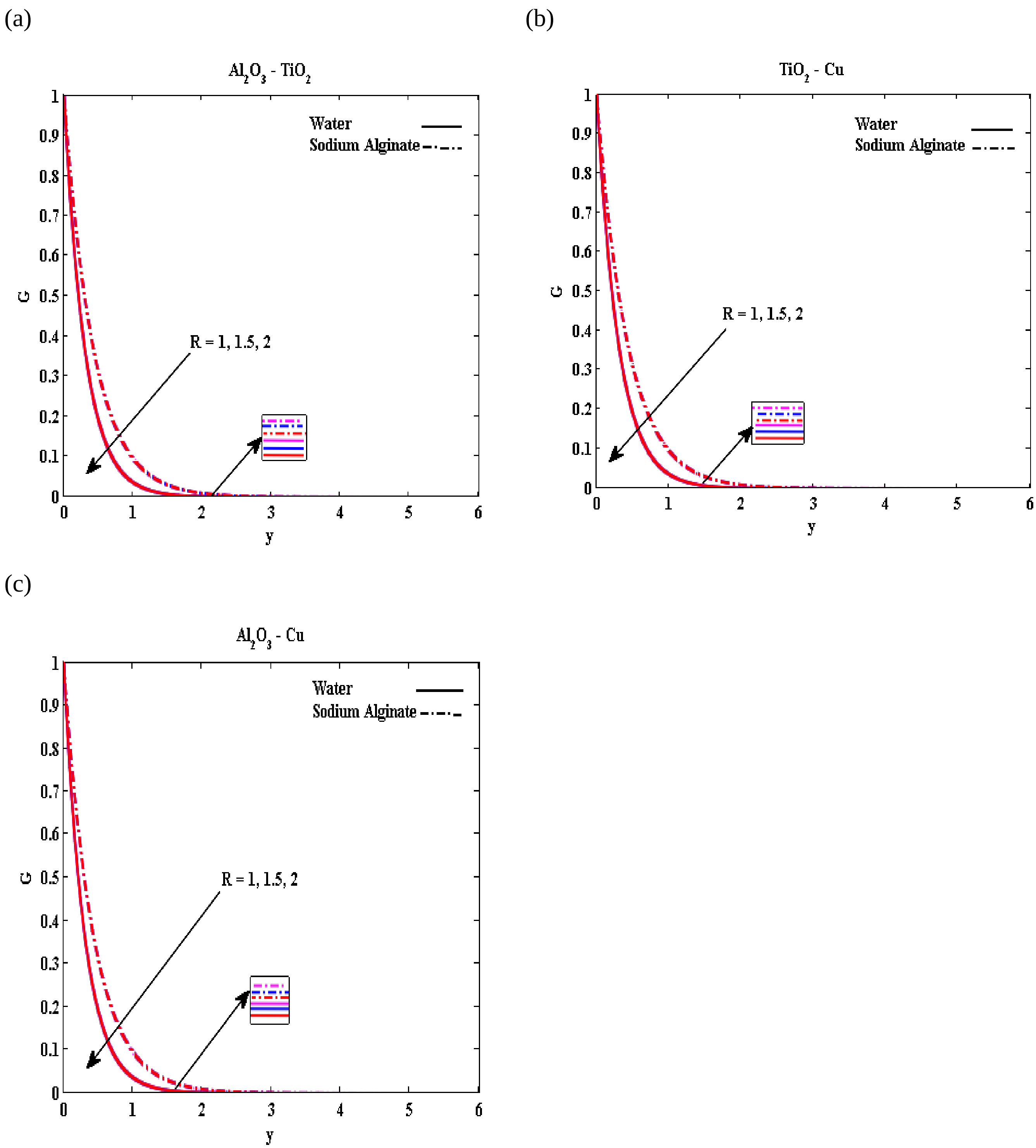

Fig.12 (a-c) Variation of R on G

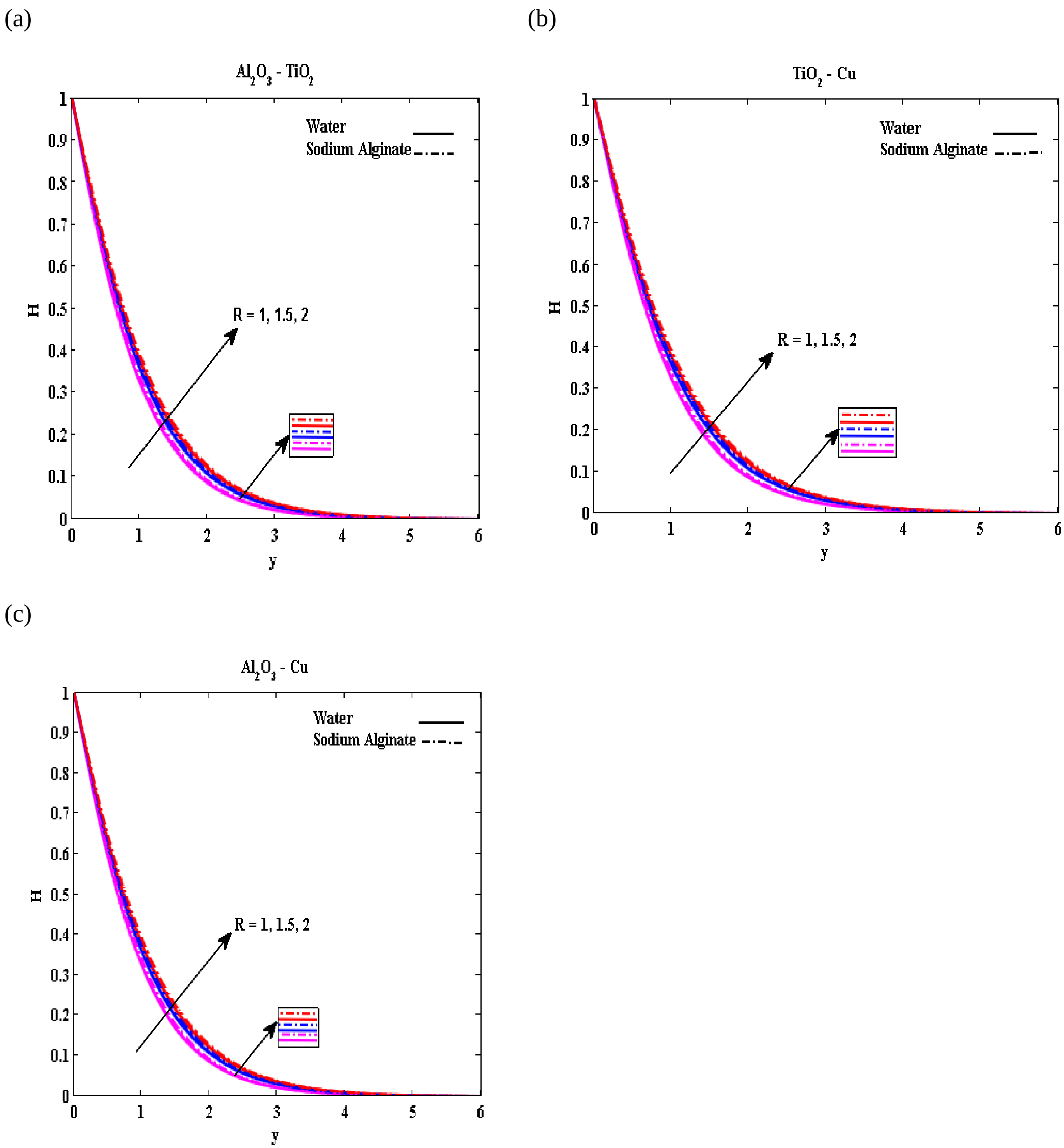

Fig.13 (a-c) Variation of R on H

(a)

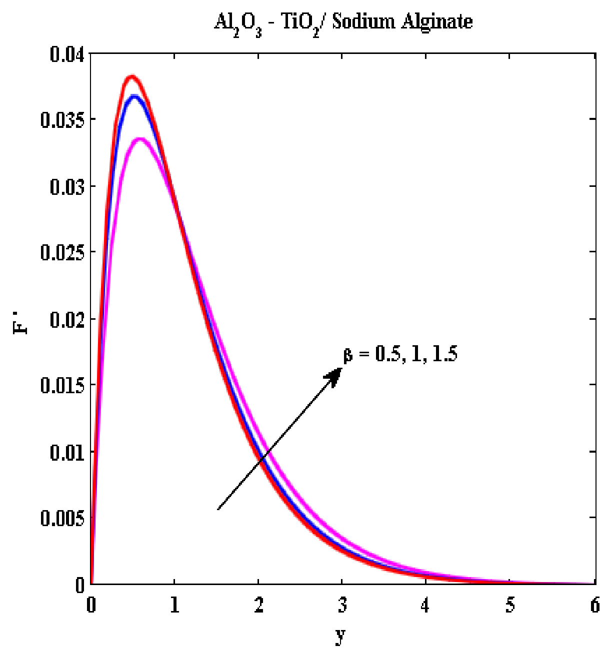

(b)

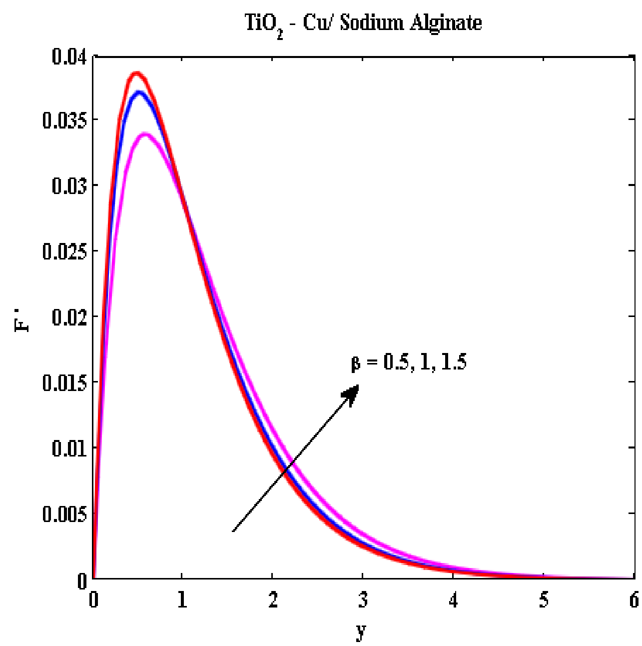

(c)

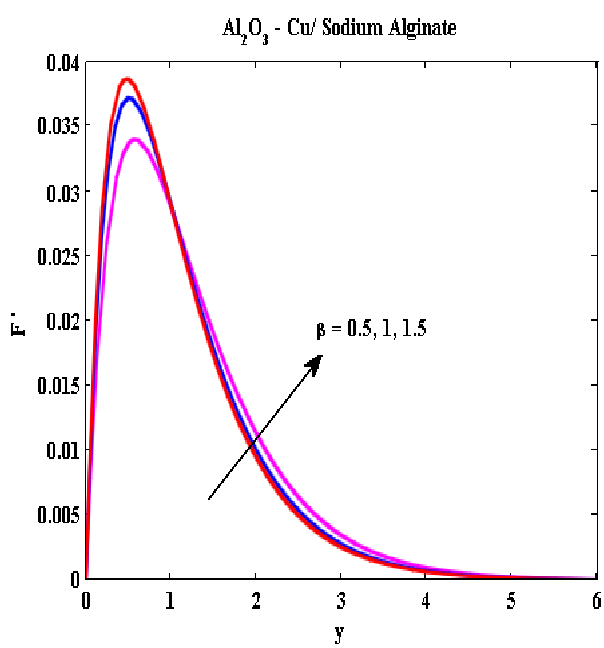

Fig.14 (a-c) Variation of β on F’

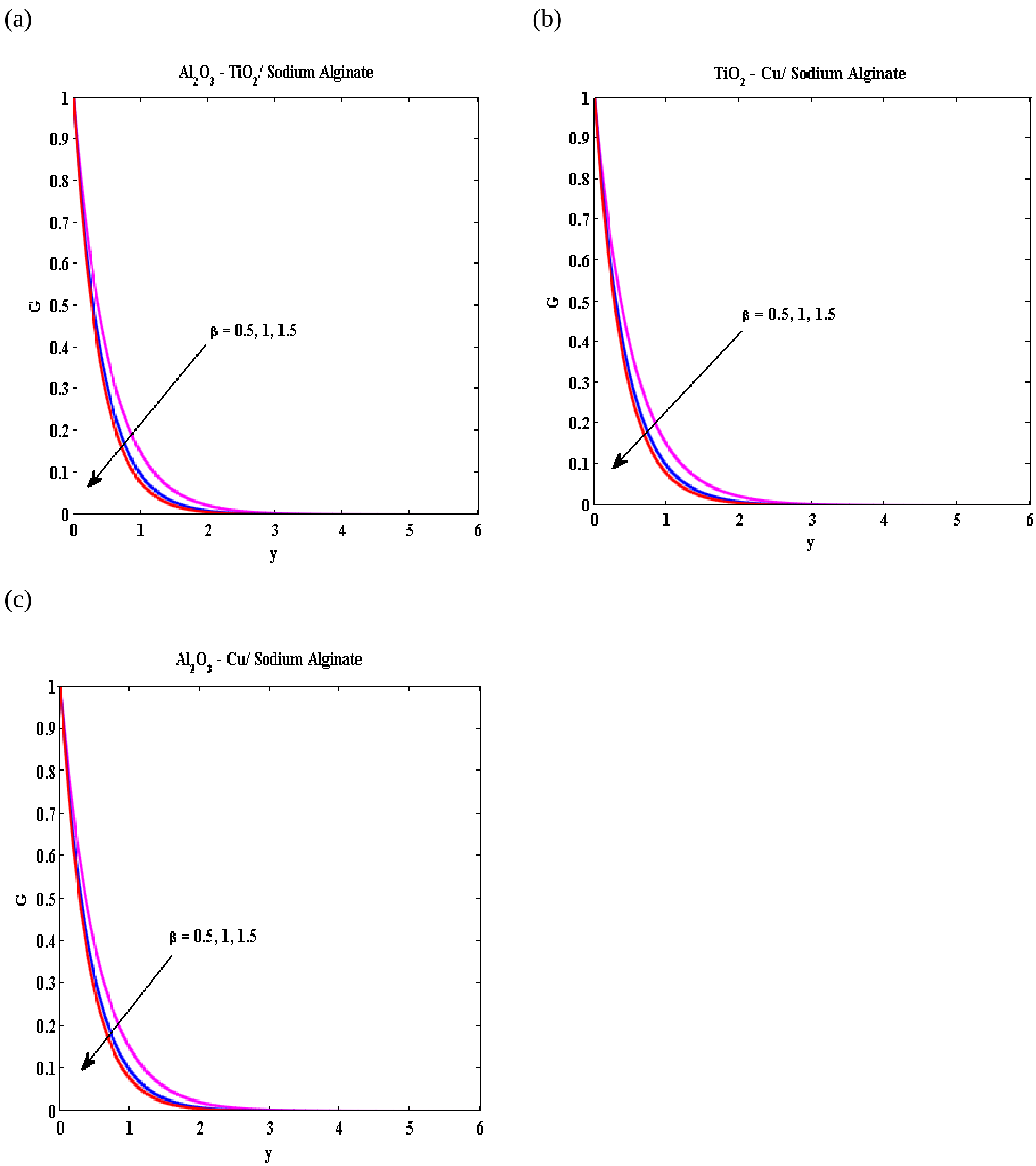

Fig.15 (a-c) Variation of β on G

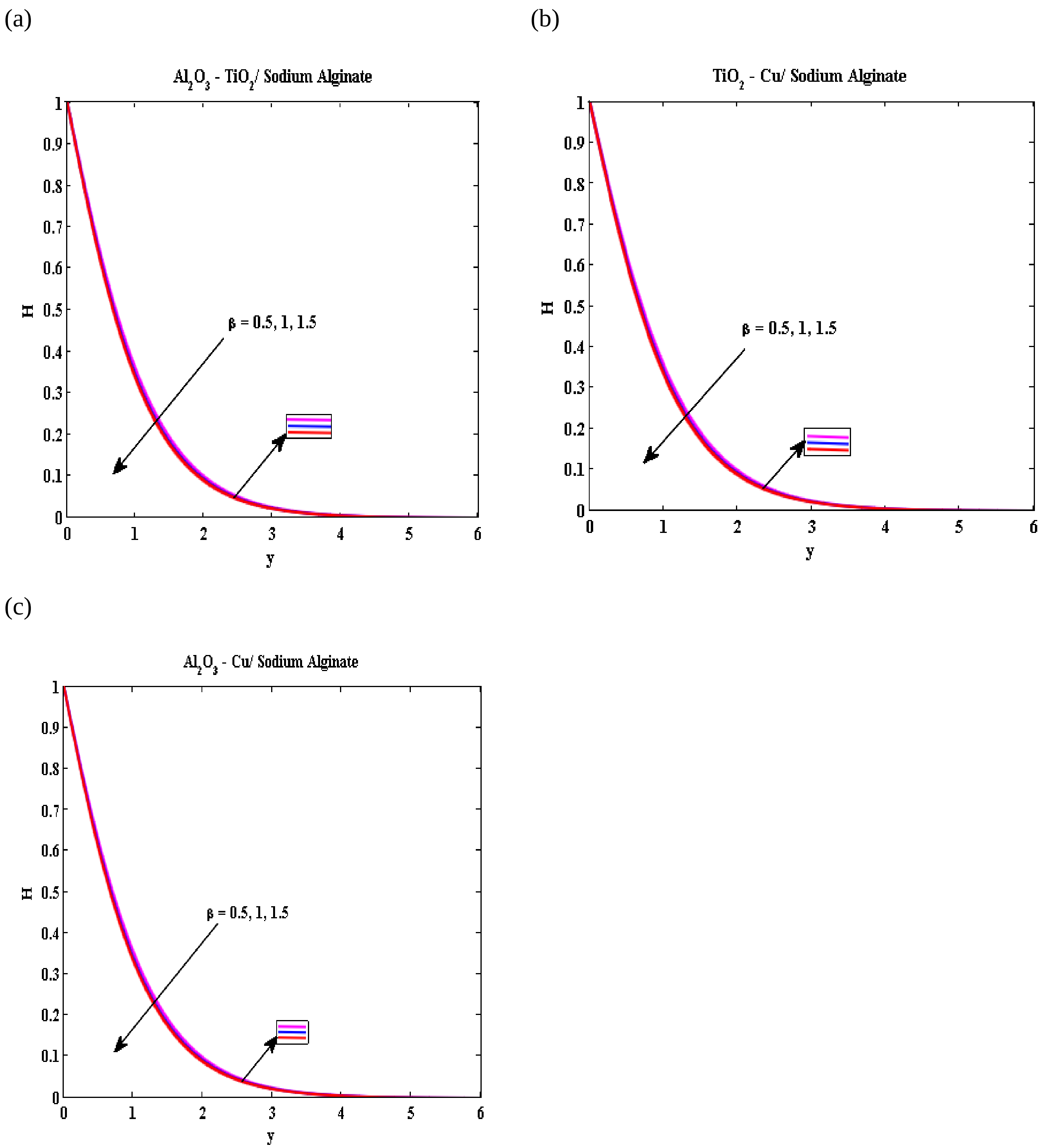

Fig.16 (a-c) Variation of β on H